Neuroscience 252 (2013) 190–200

DEVELOPMENTAL AND HYPOXIA-INDUCED CELL DEATH SHARE COMMON ULTRASTRUCTURAL AND BIOCHEMICAL APOPTOTIC FEATURES IN THE CENTRAL NERVOUS SYSTEM

V. M. POZO DEVOTO, M. E. BOGETTI AND S. FISZER DE PLAZAS *

Institute of Cell Biology and Neuroscience, Prof. E. De Robertis, School of Medicine, University of Buenos Aires, Buenos Aires, Argentina

Abstract—Hypoxic insults during the perinatal period lead to motor and cognitive impairments that later appear during childhood. In the adult brain, hypoxic events often lead to necrotic neuronal death, depending on the region and intensity of the event. During development an active apoptotic cell death occurs and could be an important variable affecting the hypoxic insult outcome. In the present work we performed a comparative study, in a chick embryo model, of the phenotypes and molecular markers exhibited during developmental and hypoxic cell death (HxCD). Ultrastructural analysis of optic tectum cells of embryos subjected to hypoxia (8% O_2, 60 min) revealed a clear apoptotic morphology that did not differ from the one exhibited during developmental cell death. Integrity of plasma membrane, condensation of chromatin in round well-defined bodies, and gradual shrinkage of the cell are all hallmarks of the apoptotic process and were present in both control and hypoxic cells. To elucidate if hypoxic and developmental cell deaths share a common mechanism we evaluated the activation of both intrinsic and extrinsic apoptotic pathways. A basal cleavage of caspase-9 and cytochrome c release was observed by co-immunofluorescence in control embryos, but hypoxic insult significantly increased the incidence of this colocalization. Caspase-8 cleavage remained unchanged after the hypoxic insult, suggesting that the extrinsic pathway would not be involved in hypoxic death. We also observed a significant decrease of Akt activation immediately after hypoxia, possibly facilitating the later release of cytochrome c. In addition we analyzed the influence of retinal ganglion cells (RGC) in neuronal survival. Transection of RGC fibers at embryonic day (ED) 3 did not induce any change in developmental and HxCD at ED12. In conclusion, our findings demonstrate that a hypoxic insult in the developing brain triggers the same apoptotic pathway as the active developmental death.

Key words: apoptosis, hypoxia, neuronal death, development, chick optic tectum.

INTRODUCTION

Hypoxia is defined as a decrease in oxygen availability for a given tissue or group of cells. In the pre and perinatal periods, hypoxic insults could lead – among other pathologies – to hypoxic ischemic (HI) encephalopathy, a relatively common condition which results in serious consequences for many of the infants including death, cerebral palsy, epilepsy and other significant cognitive, developmental and behavioral problems (Kurinczuk et al., 2010; Northington et al., 2011). In general terms hypoxic events have a better prognosis than HI events. Nevertheless many studies have shown important changes derived from hypoxia such as altered corticogenesis (Ment et al., 1998), decreased number of neurons and glial cells (Schwartz et al., 2004), damaged white matter (Baud et al., 2004) and impaired neuronal processes development and connections (Rees et al., 1998). Apoptotic, necrotic and hybrid phenotypes have been observed in both hypoxic and HI events (Busl and Greer, 2010). Although necrosis is the most frequent phenotype in HI events (Martin et al., 1998), apoptotic cell death is present in regions where blood flow is less significantly reduced (e.g. penumbra).

The specific regional vulnerability and the magnitude of the damage of a hypoxic event in the prenatal brain change during development, due to the constant reorganization of the CNS including processes as proliferation, migration, differentiation and cell death. Neuronal death during CNS development is known as naturally occurring cell death (NOCD), and is phylogenetically conserved and present in every structure of the CNS (Glücksmann, 1951). This developmental neuronal death is mainly apoptotic, but autophagocytic and necrotic cell death can also be observed (Schweichel and Merker, 1973). Understanding the mechanism of hypoxic cell death (HxCD) execution during perinatal periods could lead to the development of neuroprotective strategies that ameliorate the outcome of hypoxic insults.

*Corresponding author. Address: Instituto de Biología Celular y Neurociencias, Prof. E. De Robertis, Facultad de Medicina, Universidad de Buenos Aires, Paraguay 2155, 1121 Buenos Aires, Argentina. Tel: +54-11-5950-9500x2078; fax: +54-11-5950-9626.
E-mail address: sfiszer@fmed.uba.ar (S. Fiszer de Plazas).

Abbreviations: C'h-i-j', cell compartment 'h-i-j'; DAB, 3,3′-diaminobenzidine tetrahydrochloride; ED, embryonic day; EDTA, ethylenediaminetetraacetic acid; HI, hypoxic ischemic; HxCD, hypoxic cell death; NOCD, naturally occurring cell death; OL, optic lobe; OT, optic tectum; PB, phosphate buffer; PBS, phosphate-buffered saline; PVDF, polyvinylidene fluoride; RGC, retinal ganglion cells; SDS, sodium dodecyl sulfate; SGC, stratum griseum superficiale; TUNEL, TdT-mediated dUTP nick-end labeling; TX-100, Triton X-100.

0306-4522/13 $36.00
http://dx.doi.org/10.1016/j.neuroscience.2013.07.065

The avian optic tectum (OT) is a bilateral mesencephalic structure that plays a key role in processing visual information (Scicolone et al., 1995). On embryonic day (ED) 12, the OT is composed of the ependyma and four embryonic cell layers constituted by neurons in the process of differentiation. The cell compartment 'h-i-j' (C'h-i-j') and the stratum griseum superficiale (SGC) are the main layers and they present differences in cytoarchitecture and connections. C'h-i-j' is a dense cell layer which receives retinal afferent input, populated with small neurons with a nucleus that occupies most of the cell. SGC – with lower density – is the first neuronal layer to be formed and is maintained through all the development process. The main efferents of the OT project to the thalamus from the large multipolar cells present in this layer.

The developing chick OT provides an excellent model to study the vulnerability to a hypoxic insult since it presents a well-known cytoarchitectural organization along with the absence of maternal variables during the hypoxic event. In a previous work we have shown that HxCD is observed 6 h after a hypoxic insult, while NOCD maintains its rate and is apparently not affected by the hypoxic insult. In that work we used three different markers of cell death none of which allowed distinguishing NOCD from HxCD. In the present work we attempted to find out whether HxCD uses the same execution pathway as the NOCD. As active caspase-3 is present in both, we comparatively studied the intrinsic and extrinsic pathway, the ultrastructural features and the influence of retinal ganglion cells (RGC) afferents in both NOCD and HxCD in the avian OT.

EXPERIMENTAL PROCEDURES

Animals and hypoxic treatment

Fertile chicken (*Gallus gallus domesticus*)-specific pathogen-free eggs from White Leghorn were obtained from a local hatchery and incubated at 38 °C and 60% relative humidity. At ED12 or stage 38 according to the criteria of Hamburger and Hamilton (1992), embryos were subjected to a global hypoxic treatment as previously described by Rodríguez Gil et al. (2000). Briefly, eggs were vertically placed in a 10 l plastic chamber inside the incubator (in the same conditions of temperature, pressure and humidity as the control eggs) and subjected to a stream of 8%O_2/92%N_2 for 60 min, at a flow rate of 1 l/min. The chamber contained retention valves to allow the escape of gases in excess while avoiding mixing with atmospheric air, and a storage space with calcium hydroxide to absorb CO_2 formed during hypoxic treatment. After normobaric hypoxic treatment, eggs were immediately processed or returned to normoxic conditions in the incubator, and allowed to recover for different times. Control animals were those embryos not subjected to the hypoxic treatment. All procedures described were performed according to guidelines approved by the Buenos Aires University's Animal Care and Use Committee and the U.S. National Institutes of Health Guide for the Care and Use of Laboratory Animals (NIH Publications No. 80-23) revised 1996. All efforts were made to minimize the number of animals used and their suffering.

Enucleation

For enucleation, a saw was used to make a window in the region of the air space of the eggshell at ED4, and the outer and inner shell membranes were completely removed. The right eye, exposed upward as a result of embryonic development, was then removed with tweezers under a stereomicroscope, the window sealed with parafilm, and then left to develop without turning in the incubator until ED12, when some embryos were subjected to hypoxia and sacrificed 6 h post-hypoxia.

Coimmunofluorescence

Chicken embryos were decapitated, their brains rapidly removed and fixed for 12 h in 4% paraformaldehyde in phosphate-buffered saline (PBS). The optic lobes (OL), composed by OT, pretectum and tegmentum, were separated from the prosencephalon and dehydrated with a graded series of ethanol, followed by immersion in xylene. Tissue blocks were embedded in paraffin and cut in 5-μm thick sections with a microtome. The OL were placed in a way that the sections across the OT were parallel to the OL longitudinal anatomical axis. Sections were rehydrated and antigen retrieval was performed by heating the sections at 95 °C in 10 mM sodium citrate buffer pH 6.0 for 40 min. Non-specific binding was blocked for 30 min with 1% goat serum in PBS/0.3%Triton X-100 (TX-100). Primary antibody: anti-active caspase-9 (1:75) and anti-cytochrome c (1:100), were diluted in PBS/0.3%TX-100, and incubated overnight at 4 °C. It was followed by Cy2-conjugated anti-rabbit antibody for active caspase-9 and Cy3-conjugated anti-mouse for cytochrome c diluted in PBS/0.3%TX-100 and incubated for 2 h at 37 °C. Sections were then stained with Hoechst 33258 for 5 min and finally mounted with fluorescent mounting medium.

TdT-mediated dUTP nick-end labeling (TUNEL)

5-μm sections were rehydrated and incubated with proteinase K for 15 min. Then they were incubated in equilibrium buffer for 10 min, followed by reaction buffer (equilibrium buffer, nucleotide mix with fluorescein-conjugated dUTPs and terminal deoxynucleotidyl transferase) for 60 min at 37 °C. The reaction was stopped with SSC 2× for 15 min, then stained with Hoechst 33258 for 5 min and finally mounted with fluorescent mounting medium.

Western blot

Chicken embryos were decapitated and OL were removed on ice and OT rapidly dissected. Then OT were homogenized in ice-cold lysis buffer (20 mM pH 8 Tris–HCl, 137 mM NaCl, 2 mM EDTA, 1% TX-100, 10% glycerol) supplemented with phosphatase inhibitors (10 mM NaF, 1 mM Na_3VO_4) and protease inhibitors (1 μM leupeptin, 1 μM aprotinin, 1 μM pepstatin A, 1 mM phenylmethanesulfonyl fluoride (PMSF)).

Homogenates were pelleted at 12,500 g for 30 min and the supernatant was collected and stored at −20 °C.

Total fractions were denatured in sodium dodecyl sulfate (SDS) loading buffer (62.5 mM Tris–HCl pH 6.8, 2% SDS, 10% b-mercaptoethanol, 10% glycerol, 0.002% bromophenol blue) at 100 °C for 10 min and then separated by electrophoresis on a SDS–polyacrylamide gel at 15%. Proteins were then transferred to a polyvinylidene fluoride (PVDF) membrane. After blocking (5% milk, 1% glycine in PBS–Tween 20 0.05%) for 1 h, membranes were incubated with the primary antibody (caspase-8, 1:600; Akt, 1:1000; pAkt, 1:700; actin, 1:1000) overnight at 4 °C followed by HRP-conjugated secondary antibodies. Bands were detected by chemiluminescence using an ECL Kit.

Electron microscopy

After decapitation, brains were removed and fixed for 12 h with 4% paraformaldehyde/0.25% glutaraldehyde in 0.1 M phosphate buffer (PB). After washing steps with PB, the OL were separated from the prosencephalon and included in agarose 4% in 0.1 M PB. Sections of 200 μm were cut using a vibratome, and a specific region of the OT was selected using a dissecting knife and a stereomicroscope. For immunohistochemistry, antigen retrieval was performed heating the floating sections at 65–70 °C in 10 mM sodium citrate buffer pH 6.0 for 30 min. Floating sections were then placed in a multi-well and non-specific binding was blocked with 5% normal goat serum in PB for 1 h in a shaker. Incubation with primary antibody was performed with anti-caspase-3 (1:60) diluted in PB for 4 days at 4 °C in a shaker. After washing, sections were blocked for peroxidase activity with 3% H_2O_2 in PB for 30 min. Secondary biotinylated anti-rabbit antibody diluted in PB was added for 3 h at room temperature in a shaker, followed by incubation with streptavidin for 2 h at room temperature. Then sections were incubated with a substrate solution of 0.05% 3,3′-diaminobenzidine tetrahydrochloride (DAB)/ 0.03% H_2O_2 in PB for approximately 8 min. Sections where immunohistochemistry was performed and those that were not, followed the routine protocol for electron microscope tissue preparation. Briefly, postfixation with 1% OsO_4 in 0.1 M pH 7.4 PB for 1 h at 4 °C was made. Following washing steps with distilled water, a counter stain with 2% Uranyl Acetate for 30 min at 4 °C was performed. Then sections were dehydrated with a graded series of ethanol and embedded with poly/bed 812. Ultramicrotome sections were cut, mounted in 300 mesh grids and stained with 1% Uranyl Acetate and Reynolds solution. Semithin ultramicrotome sections of 0.5–1 μm were stained with Toluidine Blue solution for 5 min, cleared and mounted in resinous mounting medium.

Image acquisition and quantification

On ED12, the OL longitudinal anatomical axis runs parallel to the developmental gradient axis. Sections were cut parallel to these axes yielding a rostral and a caudal pole. As the rostral side is ahead in development, to get rid of any developmental variable we made all measurements halfway between the rostral and the caudal poles.

Images were taken with an Olympus BX50 microscope (Olympus, Tokyo, Japan) and acquired with a CCD camera and ImagePro Plus software (Media Cybernetics Inc.). For TUNEL+ cells counting, whole OT mosaics were made from 200× images. Four sections were analyzed and averaged for each experimental unit. For colocalization of cleaved caspase-9 and cytosolic cytochrome c, 400× images corresponding to the different layers were acquired from eight sections and averaged for each experimental unit. To get rid of any density bias, the number of colocalizing cells for each image was normalized to the total number of nuclei. Quantification and morphological analysis were performed with the ImageJ software.

For Western Blot analysis, optical density was quantified with Gel-Pro Analyser, version 3.1 (Media Cybernetics Inc., Bethesda, MD, USA).

All the statistical analysis was performed using GraphPad Prism version 4.00 for Windows, GraphPad Software, San Diego, CA, USA.

Antibodies and markers

Polyclonal antibody against p17 subunit of the active caspase-3, polyclonal antibody against p37 subunit of active caspase-9, monoclonal antibody against cytochrome c and monoclonal antibody against actin were purchased from Chemicon International, Temecula, CA, USA. Polyclonal antibody against pAkt (Ser473) and polyclonal antibody against Akt were purchased from Cell Signaling, Danvers, MA, USA. Polyclonal antibody against p18 subunit of caspase-8 was purchased from Santa Cruz, CA, USA. Secondary Cy2-conjugated anti-rabbit and Cy3-conjugated anti-mouse antibodies were from Chemicon International and secondary biotinylated anti-rabbit antibody was obtained from Dako Cytomation, Carpinteria, CA, USA. Streptavidin and DAB was from Sigma, St. Louis, MO, USA. Hoechst stain 33258 was from Sigma and TUNEL kit was from Promega Corporation, Madison, USA. Fluorescent Mounting Medium was from Dako Cytomation. Acrylamide was obtained from Bio-Rad, Richmond, CA, USA, PVDF membranes obtained from Millipore Corporation, Bedford, MA, USA and ECL Kit was from Amersham Pharmacia Biotech, Piscataway, NJ, USA.

RESULTS

Ultrastructural analysis

We have previously found that a hypoxic insult on the developing OT increases the total number of dead cells 6 h post-hypoxia, but none of the markers used allowed distinguishing NOCD from HxCD (Pozo Devoto et al., 2006). To clarify whether both NOCD and HxCD share a common mechanism of death, we performed an ultrastructural analysis in OT sections from ED12 embryos subjected to hypoxia followed by 6 h of normoxic recovery. The first observation was that both

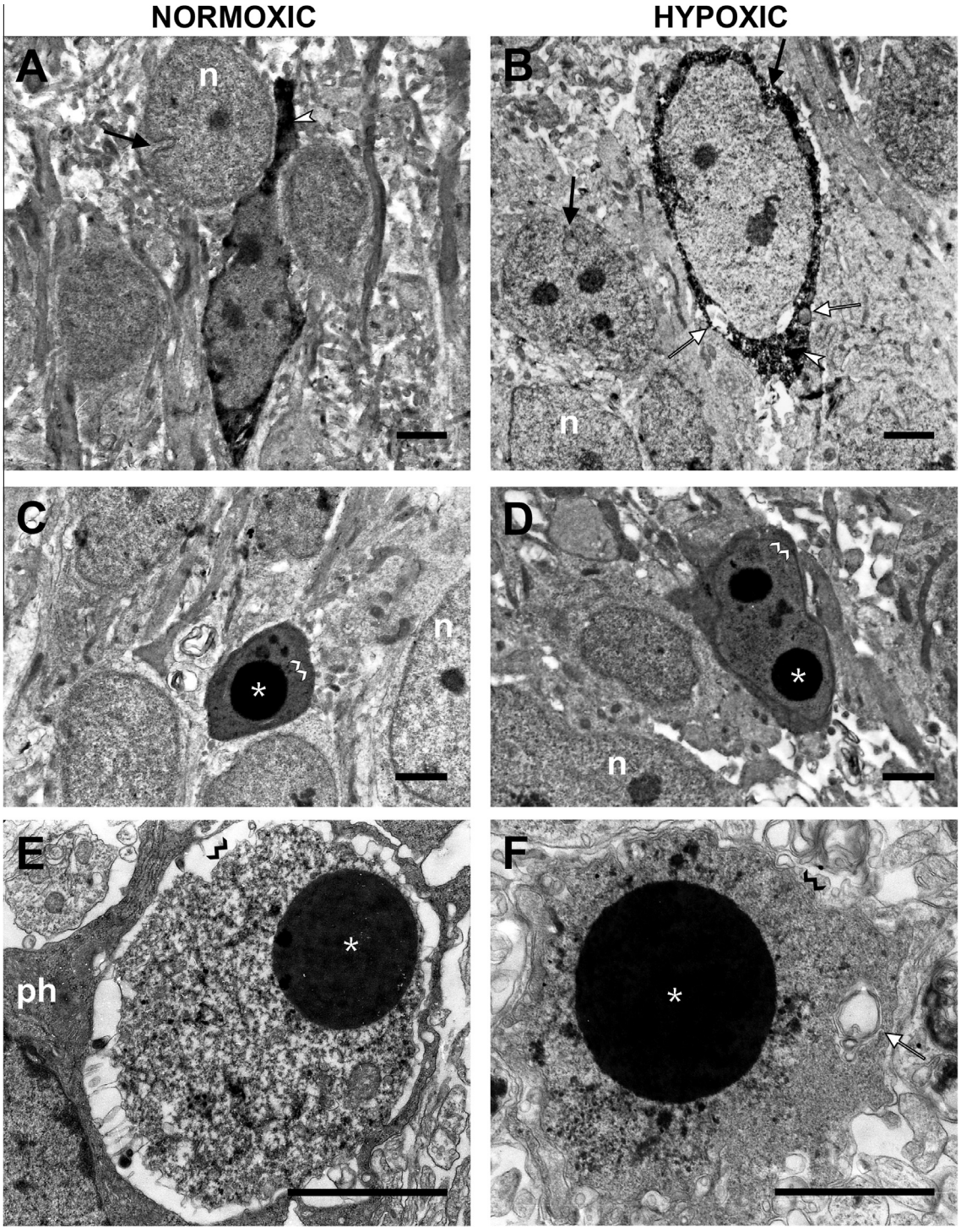

Fig. 1. NOCD and HxCD share a common apoptotic ultrastructural degeneration. Ultramicrophotographs showing the typical degeneration progress of neurons of layer C'h-i-j' at ED12 for both normoxic (A, C, E) and hypoxic embryos (B, D, E). The degenerative process is divided in three stages: early (A, B), middle (C, D) and late (E, F). (A, B) OT sections subjected to immunohistochemistry with anti-caspase-3 to detect early changes. Nuclei show a nearly normal shape with mild chromatin condensation, nucleoli and a few nuclear indentations (black arrow) are present in both normal (n) and degenerating cells. Organelle swelling (white arrow) and vacuoles are present in the dark caspase-3 stained cytoplasm (white arrowhead). (C, D) Degenerating cells shrink and darken, whereas the nuclear envelope is still intact (double white arrowhead), separating the nuclear from the cytosolic compartments. Chromatin condenses in large round aggregates (asterisk) and the cytoplasm presents a homogeneous particulate. (E, F) In this final stage, the cell continues shrinking and the nuclear–cytoplasmic division is lost. The round chromatin aggregates increase in size and density. In this stage, the cells are often engulfed by a phagocytic cell (ph). Important to note is the integrity of the plasma membrane during all the processes (double black arrowhead). Scale bar = 2 μm.

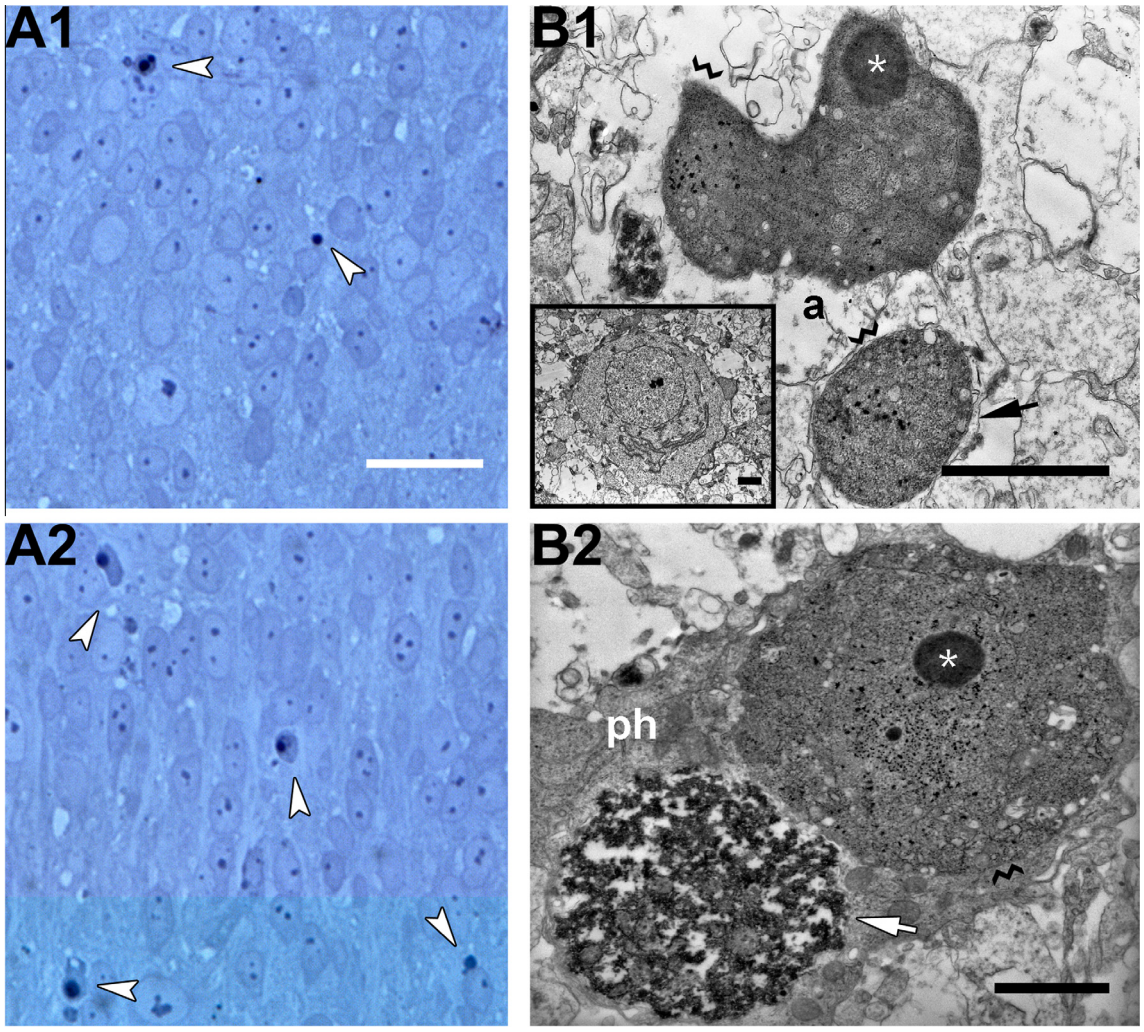

Fig. 2. Apoptotic degeneration is observed throughout the OT in NOCD and HxCD. Semi thin sections of layer C'h-i-j' (A) and apoptotic morphology present in layer SGC (B) of OT on ED12 in both the normoxic (A1, B1) and the hypoxic (A2, B2) treatments. (A) Toluidine Blue-stained semithin sections of layer C'h-i-j' of the OT, showing the increase in apoptotic figures (arrowheads) 6 h after the hypoxic treatment (A2) compared to normoxic embryos (A1). (B) Ultramicrographs of apoptotic figures present in normoxic (B1) or hypoxic (B2) embryos in layer SGC of the OT. The late stage of degeneration is depicted, showing cell shrinkage, a well-defined plasma membrane (double arrowheads), chromatin condensation (asterisk) and astrocytic (a) or phagocytic cell (ph) engulfment. Also, compare somatic degenerating body (B1, black arrow) vs. neuronal process degeneration (B2, white arrow). inset in B1. Normal morphology of a typical SGC cell. These multipolar neurons are larger and present a well-developed cytoplasm when compared to C'h-i-j' neurons. Also, their density is lower. Scale bar = 20 μm (A), 2 μm (B).

normoxic and HxCD showed classic apoptotic morphology in all the OT layers (Figs. 1 and 2). An increase in cell death was observed after the hypoxic treatment (Fig. 2A), while the apoptotic morphology was observed for both C'h-i-j' and SGC layers in normoxic or hypoxic treatment. None of the OT layers analyzed showed necrotic morphology. We divided the degenerative process into three successive stages. In the early stage, the nucleus showed a nearly normal morphology and nucleoli were present, chromatin began to condense faintly staining the nucleoplasm (Fig. 1A, B). Nuclear envelope indentations were observed but were also present in normal cells (both normoxic and hypoxic). Given the difficulty to identify this stage, we performed immunohistochemistry against active caspase-3, which was observed as an electrondense patch in the cytosol. Also in this stage organelle swelling and vacuole formation were observed. The next stage was characterized by a marked decrease in cell size and evident nuclear changes: chromatin condensed and aggregated in large round masses, a classic apoptotic hallmark (Fig. 1C, D), whereas the nuclear membrane remained intact, dividing the nuclear from the cytosolic compartment. The cytosol presented a homogenous particulate probably due to ribosomal disaggregation, and a continuous plasma membrane separated the cell from the external medium. In the late stage the nuclear membrane was lost, the cell continued shrinking, and chromatin aggregates became larger and more electrondense (Fig. 1E, F). Degenerating organelles were still present and phagocytic cells were typically found engulfing these bodies. This process detailed for C'h-i-j' layer (Fig. 1.) was equally present in the SGC layer (Fig. 2B).

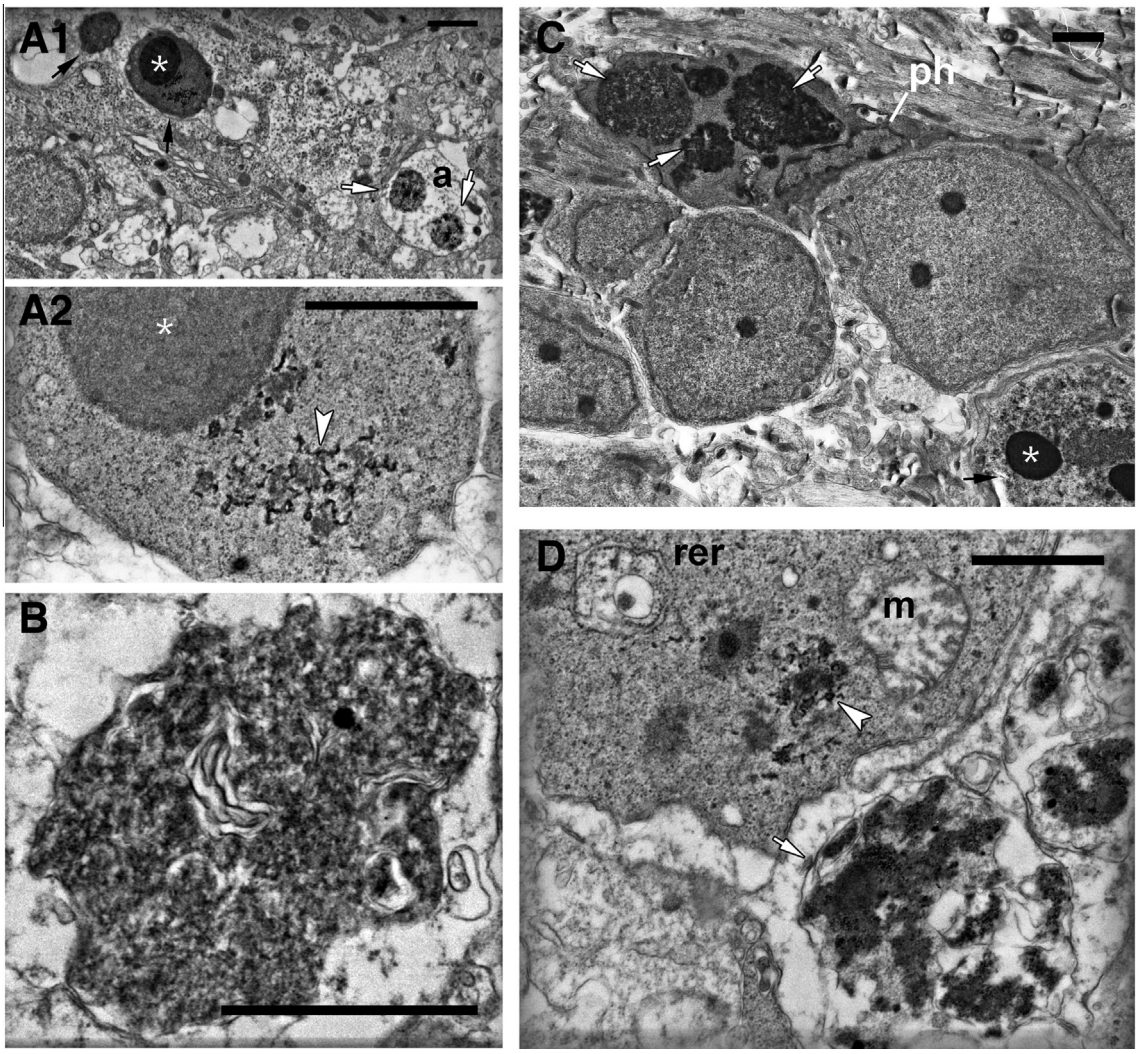

Fig. 3. Neuronal process degeneration morphology and particle aggregation. Ultramicrophotographs showing morphological features of both normoxic and hypoxic neuronal death. (A1) Apoptotic cell that presents four bodies, two of them being part of the soma (black arrow) (magnified in A2), while two processes degenerating (white arrow) are engulfed by an astrocytic process (a). (A2) Electrondense particles aggregates (white arrowhead) observed in apoptotic bodies corresponding to the soma. (B) Small body of electrondense material intercalated by membrane folds characteristic of process degradation morphology. Note the absence of homogeneously faintly gray-stained cytosol. (C) A degenerating soma (lower right) and a process (upper left) engulfed by a phagocytic cell (ph). (D) Soma with swollen mitochondrion (m) with poorly defined cristae and a vacuole of rough endoplasmic reticulum (rer). Also electron dense particles aggregates and process degeneration is present. Scale bar = 2 μm (A1, C); 1 μm (A2, B, D).

Ultrastructural features

Later stages of cell demise frequently showed electrondense particles in the shape of short strings or aggregates present in the cytosol (Fig. 3A2, D). This was particularly evident in hypoxic embryos, and sections stained only with Uranile Acetate (without OsO_4) suggest that they were mainly composed of protein or ribonucleoprotein (data not shown).

Neurons were morphologically divided into the soma and process or neurites. We found that degeneration of the soma was different from the process degeneration (Fig. 3A1, C, D). The processes of normal neurons look continuous, without segmentations, whereas degenerated ones are segmented in round bodies that separate from each other like collar beads (Fig. 3A1). These beads were often observed in the expected direction of the neuron's process and specifically were not buds of the soma. Also their composition differed from that of the soma. The former presented electrondense patches mixed with membrane foldings and a limiting membrane difficult to follow (Fig. 3B), while the latter had a faintly gray-stained cytosol; organelles, vacuoles and round chromatin condensation were frequently present and the body was limited by a continuous membrane.

Role of OT afferent fibers in hypoxia

Glutamatergic fibers from the RGC are largely the main afferents of the OT, reaching the OT around ED8 and covering it completely by ED12. To study the RGC fibers influence on NOCD and HxCD on ED12, we dissected the right eye on ED4. Embryos were left to

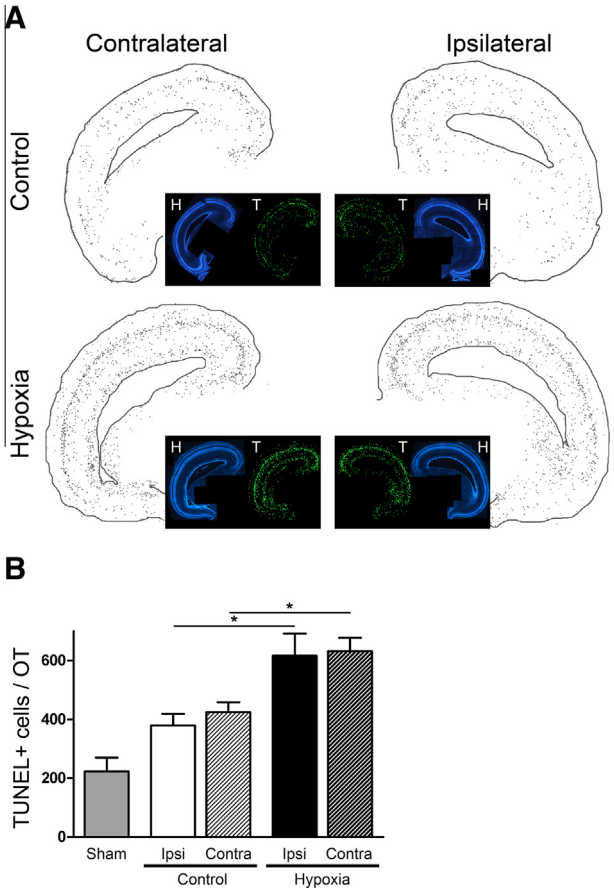

Fig. 4. RGC's fibers do not influence OT cell death on ED12. Embryos subjected to unilateral enucleation on ED4 were left to develop until ED12. A group was subjected to a hypoxic treatment and normoxic recovery for 6 h. Sections of the OT were stained with Hoechst and a TUNEL reaction performed. (A) Whole OT camera lucida drawings of photographic mosaics, where the TUNEL + cells for ipsi or contralateral sides of normoxic or hypoxic embryos are shown. Inset: OT stained with Hoechst (H) or TUNEL (T) corresponding with each drawing. (B) Quantitative analysis of TUNEL + cells per OT. Neither the control nor the hypoxic embryos show significant differences between the ipsi and the contralateral sides (Ipsi vs. Contra: C, 379 ± 39 vs. 424 ± 34; Hx, 617 ± 74 vs. 632 ± 44). The hypoxic treatment produces a significant increase in both sides when compared to control. A one-way ANOVA followed by a Bonferroni post-test was performed. Values are expressed as means ± SEM of four independent experiments. $^{*}P < 0.05$.

develop and on ED12 some embryos were subjected to hypoxia followed by 6 h of normoxic recovery, while control embryos were maintained in normoxic air. Whole OT TUNEL+ cells were counted (Fig. 4). No significant differences in TUNEL+ cells were found between ipsilateral and contralateral OT in either treatment, i.e. with or without hypoxia. On the other hand, hypoxia increased cell death levels on ED12 independently of the presence or absence of RGC fibers.

Intrinsic and extrinsic pathways

To evaluate the effect of the hypoxic insult on the PI3K/Akt survival pathway, Akt activation was analyzed on OT sections at early post-hypoxia times and in a hypoxic treatment of 30 min (Fig. 5A). The results showed a significant decrease in pAkt levels after 1 h of hypoxia (but not at 30 min of hypoxia), recovering gradually to control levels at 30 and 90 min after hypoxia.

Both in electron microscopy results of this study and previous results show a robust activation of caspase-3 at 6 h post-hypoxia which is related to degenerating cells, not only in the hypoxic treatment but also in NOCD. To evaluate the pathway responsible for caspase-3 activation, we tested molecular markers for the intrinsic (cytochrome c release and caspase-9 activation) and extrinsic (caspase-8 activation) pathways.

Co-immunofluorescence performed on OT sections from normoxic and hypoxic embryos, showed that a diffuse cytosolic presence of cytochrome c colocalizes with caspase-9 activation (Fig. 5B). Quantification of these cells after hypoxia, revealed a significant increase in the number of colocalizing cells 4 h post-hypoxia. Together with previous observations, this result confirms a temporal evolution where cytochrome c and caspase-9 activation precedes caspase-3 activation after the hypoxia. Also, normoxic levels of colocalizing cells equaled normoxic levels of cells with caspase-3 activation, suggesting that NOCD is executed by the intrinsic pathway.

To analyze caspase-8 activation, we performed a Western Blot on OT from embryos at different post-hypoxia times (Fig. 5C). The antibody against caspase 8 revealed two different forms: p55, which is the full inactive form of caspase-8 or procaspase and p18, which is a subunit of the full form cleaved after caspase-8 activation. Quantification of both forms, showed no significant variation at any of the post-hypoxia times when compared to normoxic levels, suggesting that the extrinsic pathway is not responsible for caspase-3 activation in HxCD.

DISCUSSION

Together with previous data (Pozo Devoto et al., 2006), results shown in the present work suggest that HxCD and NOCD share a common execution pathway in the avian CNS, which is not only morphologically identical but also compromises the same biochemical triggers. The apoptotic phenotype is not surprising for a NOCD process, in fact the vast majority of programed cell death of the developing CNS – not only among vertebrates but also among invertebrates – occurs by this mechanism (Kerr et al., 1972; Blaschke et al., 1996; Shaham and Horvitz, 1996; Miller and Kaplan, 2001). Nevertheless, in rodent paradigms neuronal death triggered by a hypoxic or ischemic event has proved to present heterogeneous phenotypes or mechanisms, depending mainly on age, structure affected, insult intensity and duration (Northington et al., 2001; McQuillen et al., 2003; Wei et al., 2004; Busl and Greer, 2010; Wang et al., 2011). The similarity between the HxCD and NOCD revealed in the present work supports the hypothesis that states the existence of a period of increased vulnerability during development (Martin et al., 1998), in which an active developmental process as programed cell death recruits more cells as a result

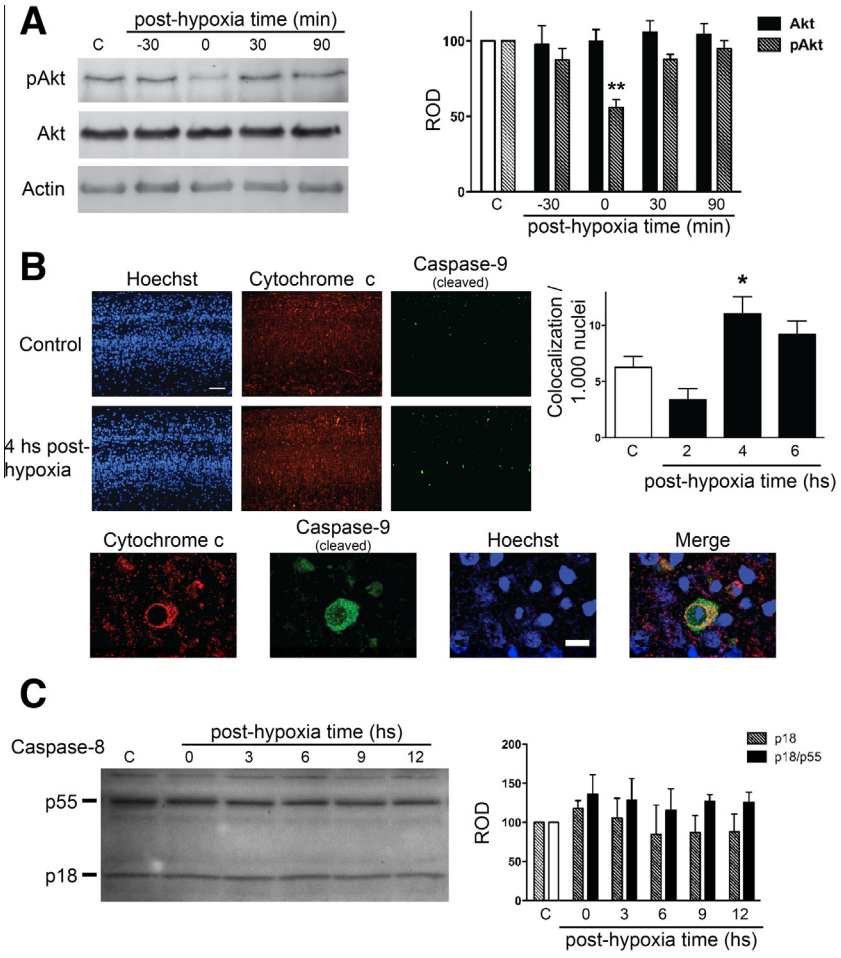

Fig. 5. Intrinsic but not extrinsic apoptotic pathway is activated after hypoxia. ED12 embryos were subjected to hypoxia and returned to normoxic condition at different times. OT were processed for Western Blot analysis of Akt/pAkt (A) and caspase-8 (C) levels and for co-immunofluorescence against cytochrome c and active caspase-9 (B). (A) pAkt levels significantly decrease immediately after hypoxia (C: 100% vs. H0: 56 ± 5%) and gradually recovers to normal levels at 30- and 90-min post-hypoxia. Total Akt does not change after the hypoxic treatment. Graph shows optical density quantification normalized to control levels of total Akt and pAkt respectively. A one-way ANOVA for Akt and pAkt was performed, followed by Dunnett's post-test comparing post-hypoxia treatments vs. control. Values are expressed as means ± SEM of six independent experiments. $^{**}P < 0.01$. (B) Colocalization of cytosolic cytochrome c (red) and active caspase-9 (green) in OT cells after hypoxic treatment. Bar graph shows the number of cells that present colocalization normalized to 1000 total cells. The number of cells showing colocalization significantly increases at 4 h post-hypoxia (C: 6.26 ± 0.97 vs. H4: 1.03 ± 1.51). A one-way ANOVA followed by Dunnett's post-test comparing post-hypoxia vs. control treatments was performed. Values are expressed as mean ± SEM of five independent experiments. $^{*}P < 0.05$. Scale bar: upper panel 50 μm, lower panel 10 μm. (C) No significant change of procaspase-8 (p55) and active caspase-8 subunit (p18) levels are observed after the hypoxic treatment. Graph shows optical density quantification normalized to control levels of p18 subunit and p18:p55 ratio respectively. A one-way ANOVA for p18 and p18:p55 ratio was performed. Values are expressed as means ± SEM of four independent experiments. (For interpretation of the references to color in this figure legend, the reader is referred to the web version of this article.)

of a temporal homeostatic disruption (e.g. reduction of O_2 availability). Furthermore, if the selective agents of NOCD are neurotrophic factors, the increased cell death observed after a hypoxic insult could be an indirect consequence: the result of a decrease in the availability of a trophic factor and not a direct effect of O_2 reduction (Young et al., 2004; Northington et al., 2005).

The ultrastructural analysis of OT layers clearly showed that not only control embryos but also embryos subjected to an acute hypoxia presented a cellular degeneration that phenotypically resembled apoptosis. Integrity of the plasma membrane, condensation of chromatin in round well-defined bodies, and gradual shrinkage of the cell (with a complete absence of swelling) are all hallmarks of the apoptotic process (Kerr et al., 1972; Majno and Joris, 1995; Martin et al., 1998). In the search for any distinction in the phenotypes present in hypoxic embryos versus normoxic embryos we found two features that were more frequent but not exclusive of HxCD: electrondense cytosolic aggregates in advanced stages of cell demise; and larger chromatin condensation bodies. As they are not exclusive, we understand that these features reflect a difference in quantity but not quality.

Neuronal process opposed to somatic degeneration in the developing brain is an observation that has not been described before. In mature brains axonal degeneration can be identified by the myelin sheet surrounding the process (Saggu et al., 2010; Barrientos et al., 2011), a feature that is not present at earlier developmental stages. The unique neuronal morphology with its variable length process poses the question of how these

processes degenerate. As they do not retract, they could segment in small bodies that are finally engulfed by phagocytic or neighboring cells. These bodies which can be confused with budding bodies of the soma have a different texture. While the degenerating soma presents a homogeneous gray stain in the medium and later stages with variable content of degenerating organelles and vesicles, processes are composed mainly of heavily electrondense patches or aggregates intermingled with membrane foldings. Also, the external membrane of the soma is continuous and evident, while the process membrane is not clearly observed and may underlie the electrondense patches. This is also evidenced by the presence of these bodies up to 10 μm or more from the degenerating soma in the expected process direction, which was confirmed with optical microscopy in a wider field.

It is generally accepted that most CNS structures present two waves of cell death that differ in location and developmental stage (Lossi and Merighi, 2003). The first wave occurs early in development and is located in or adjacent to the ventricular zone; in this process some of the neuroblasts in active proliferation die. The mechanism that underlies this phenomenon, which in the OT occurs between ED5 and ED8 (Zhang and Galileo, 1998) is not clearly understood. The second wave is called neurotrophic. Many studies have established that the supply of anterograde or retrograde (from afferents or targets, respectively) factors is necessary for neuronal survival (Altar and DiStefano, 1998; Davies, 2003). As afferent retinal fibers cover the OT completely by ED12 (McLoon, 1985) we hypothesized that these fibers could be involved not only in the mild NOCD present at ED12, but also in HxCD, by means of a higher requirement of neurotrophic factors by OT cells or by a temporal decrease in factors provided by the RGC during hypoxia (Herzog et al., 1994; Garner et al., 1996). Another hypothesis includes excitotoxicity: RGC fibers are mainly glutamatergic (McGraw and McLaughlin, 1980) and depolarizations triggered by hypoxia in RGC could lead to an increase in glutamate release and consequent death. In support of this, Catsicas et al. (1992) have demonstrated that RGC's axonal transport disruption or action potential blockade derive in OT neuronal death. Surprisingly, the enucleation experiment clearly showed that RGC fibers are not only not mediating HxCD but also that they are not regulating NOCD at ED12, discarding any influence of RGC on tectal cells by ED12. However these results do not reject the possibility that autocrine or paracrine trophic factors support could be mediating both NOCD and HxCD at ED12. Unpublished observations in our laboratory describe a significant increase in OT NOCD between ED14 and ED16, probably corresponding to the second wave. It would be interesting to test the enucleation at these developmental stages.

Apoptosis (Nakajima et al., 2000), autophagocytosis (Ginet et al., 2009), necrosis (Northington et al., 2001), or even the relatively recent programed necrosis (Wang et al., 2011) are all mechanisms that have been reported in HI insults. These differences can be attributed mainly to the heterogeneity of the experimental models used, and present a major difficulty at designing a neuroprotective strategy. In our model where oxygen is the only variable affected, we observed a temporal activation of the intrinsic pathway: cytochrome c release and caspase-9 cleavage significantly increased 4 h after the hypoxic insult. This temporal profile is in accordance and precedes caspase-3 activation profile seen in a previous work (Pozo Devoto et al., 2006). Also the total number of cells for both cases is similar, strongly suggesting that the intrinsic pathway is involved in HxCD. The caspase-8 activation experiment supports this conclusion: procaspase and active subunit levels are not significantly modified after hypoxia. On the other hand, basal levels of cytochrome c release and caspase-9 cleavage seen in normoxic embryos correlates quantitatively with caspase-3 cleavage, suggesting that NOCD also occurs by the intrinsic pathway. According to this observation, there is scarce evidence for extrinsic pathway activation during development in the CNS (Segura et al., 2007). Taken together, our results support the hypothesis that apoptotic outcomes after a hypoxic/ischemic insult are favored in perinatal brains (Martin et al., 1998; Fujikawa, 2000), due primarily to the active cell death process during development.

In a preliminary approach to unveil intrinsic pathway activation we studied the PI3K/Akt survival pathway. Akt is reported to affect activation levels of a plethora of proteins involved in life and death decisions: caspase-9 (Cardone et al., 1998), Bad (Datta et al., 1997), GSK (Cross et al., 1995), Mdm2 (Mayo and Donner, 2001), NFkb (Kane et al., 1999) and FOXO (Brunet et al., 1999), among others. Akt serves as a link between neurotrophic factors and these proteins, and PI3K activation by tyrosine kinase receptors leads to increased pAkt levels. Many studies have shown that the Akt pathway is robustly activated after HI insults, thus rescuing neurons that are otherwise committed to die (Ouyang et al., 1999; Kamada et al., 2007). Our observation of a temporally discrete decrease in pAkt levels immediately after the hypoxia, supports the involvement of Akt in the cellular death cascade, by turning off the survival signal for a discrete temporal window (Luo et al., 2003). In our results there is no sign of rescuing response but rather a shut down response. Decreased levels of pAkt could lead to the intrinsic pathway activation present at 4 h post-hypoxia, subsequent caspase-3 activation and neuronal death.

CONCLUSIONS

Results shown in the present work suggest that a hypoxic insult during development leads to an apoptotic cell death which is not only morphologically identical but also compromises the same biochemical triggers as the active developmental cell death.

Acknowledgements—The authors gratefully acknowledge the expert technical assistance of Mrs. Margarita Lopez and Mrs. Mariana Lopez Ravasio. This research was supported by grants from

National Research Council PIP 0091 and National Agency for the Promotion of Scientific and Technological Development PICT 38234.

REFERENCES

Altar CA, DiStefano PS (1998) Neurotrophin trafficking by anterograde transport. Trends Neurosci 21:433–437.

Barrientos SA, Martinez NW, Yoo S, Jara JS, Zamorano S, Hetz C, Twiss JL, Alvarez J, Court FA (2011) Axonal degeneration is mediated by the mitochondrial permeability transition pore. J Neurosci 31:966–978.

Baud O, Daire J-L, Dalmaz Y, Fontaine RH, Krueger RC, Sebag G, Evrard P, Gressens P, Verney C (2004) Gestational hypoxia induces white matter damage in neonatal rats: a new model of periventricular leukomalacia. Brain Pathol 14:1–10.

Blaschke AJ, Staley K, Chun J (1996) Widespread programmed cell death in proliferative and postmitotic regions of the fetal cerebral cortex. Development 122:1165–1174.

Brunet A, Bonni A, Zigmond MJ, Lin MZ, Juo P, Hu LS, Anderson MJ, Arden KC, Blenis J, Greenberg ME (1999) Akt promotes cell survival by phosphorylating and inhibiting a Forkhead transcription factor. Cell 96:857–868.

Busl KM, Greer DM (2010) Hypoxic–ischemic brain injury: pathophysiology, neuropathology and mechanisms. NeuroRehabilitation 26:5–13.

Cardone MH, Roy N, Stennicke HR, Salvesen GS, Franke TF, Stanbridge E, Frisch S, Reed JC (1998) Regulation of cell death protease caspase-9 by phosphorylation. Science 282:1318–1321.

Catsicas M, Péquignot Y, Clarke PG (1992) Rapid onset of neuronal death induced by blockade of either axoplasmic transport or action potentials in afferent fibers during brain development. J Neurosci 12:4642–4650.

Cross DA, Alessi DR, Cohen P, Andjelkovich M, Hemmings BA (1995) Inhibition of glycogen synthase kinase-3 by insulin mediated by protein kinase B. Nature 378:785–789.

Datta SR, Dudek H, Tao X, Masters S, Fu H, Gotoh Y, Greenberg ME (1997) Akt phosphorylation of BAD couples survival signals to the cell-intrinsic death machinery. Cell 91:231–241.

Davies AM (2003) Regulation of neuronal survival and death by extracellular signals during development. EMBO J 22:2537–2545.

Fujikawa DG (2000) Confusion between neuronal apoptosis and activation of programmed cell death mechanisms in acute necrotic insults. Trends Neurosci 23:410–411.

Garner AS, Menegay HJ, Boeshore KL, Xie XY, Voci JM, Johnson JE, Large TH (1996) Expression of TrkB receptor isoforms in the developing avian visual system. J Neurosci 16:1740–1752.

Ginet V, Puyal J, Clarke PGH, Truttmann AC (2009) Enhancement of autophagic flux after neonatal cerebral hypoxia–ischemia and its region-specific relationship to apoptotic mechanisms. Am J Pathol 175:1962–1974.

Glücksmann A (1951) Cell deaths in normal vertebrate ontogeny. Biol Rev 26:59–86.

Hamburger V, Hamilton HL (1992) A series of normal stages in the development of the chick embryo. Dev Dyn 195:231–272.

Herzog KH, Bailey K, Barde YA (1994) Expression of the BDNF gene in the developing visual system of the chick. Development 120:1643–1649.

Kamada H, Nito C, Endo H, Chan PH (2007) Bad as a converging signaling molecule between survival PI3-K/Akt and death JNK in neurons after transient focal cerebral ischemia in rats. J Cereb Blood Flow Metab 27:521–533.

Kane LP, Shapiro VS, Stokoe D, Weiss A (1999) Induction of NF-kappaB by the Akt/PKB kinase. Curr Biol 9:601–604.

Kerr JF, Wyllie AH, Currie AR (1972) Apoptosis: a basic biological phenomenon with wide-ranging implications in tissue kinetics. Br J Cancer 26:239–257.

Kurinczuk JJ, White-Koning M, Badawi N (2010) Epidemiology of neonatal encephalopathy and hypoxic–ischaemic encephalopathy. Early Human Dev 86:329–338.

Lossi L, Merighi A (2003) In vivo cellular and molecular mechanisms of neuronal apoptosis in the mammalian CNS. Prog Neurobiol 69:287–312.

Luo HR, Hattori H, Hossain MA, Hester L, Huang Y, Lee-Kwon W, Donowitz M, Nagata E, Snyder SH (2003) Akt as a mediator of cell death. Proc Natl Acad Sci U S A 100:11712–11717.

Majno G, Joris I (1995) Apoptosis, oncosis, and necrosis. An overview of cell death. Am J Pathol 146:3–15.

Martin LJ, Al-Abdulla NA, Brambrink AM, Kirsch JR, Sieber FE, Portera-Cailliau C (1998) Neurodegeneration in excitotoxicity, global cerebral ischemia, and target deprivation: a perspective on the contributions of apoptosis and necrosis. Brain Res Bull 46:281–309.

Mayo LD, Donner DB (2001) A phosphatidylinositol 3-kinase/Akt pathway promotes translocation of Mdm2 from the cytoplasm to the nucleus. Proc Natl Acad Sci U S A 98:11598–11603.

McGraw CF, McLaughlin BJ (1980) Fine structural studies of synaptogenesis in the superficial layers of the chick optic tectum. J Neurocytol 9:79–93.

McLoon SC (1985) Evidence for shifting connections during development of the chick retinotectal projection. J Neurosci 5:2570–2580.

McQuillen PS, Sheldon RA, Shatz CJ, Ferriero DM (2003) Selective vulnerability of subplate neurons after early neonatal hypoxia-ischemia. J Neurosci 23:3308–3315.

Ment LR, Schwartz M, Makuch RW, Stewart WB (1998) Association of chronic sublethal hypoxia with ventriculomegaly in the developing rat brain. Brain Res Dev Brain Res 111:197–203.

Miller FD, Kaplan DR (2001) Neurotrophin signalling pathways regulating neuronal apoptosis. Cell Mol Life Sci 58:1045–1053.

Nakajima W, Ishida A, Lange MS, Gabrielson KL, Wilson MA, Martin LJ, Blue ME, Johnston MV (2000) Apoptosis has a prolonged role in the neurodegeneration after hypoxic ischemia in the newborn rat. J Neurosci 20:7994–8004.

Northington FJ, Chavez-Valdez R, Martin LJ (2011) Neuronal cell death in neonatal hypoxia–ischemia. Ann Neurol 69:743–758.

Northington FJ, Ferriero DM, Graham EM, Traystman RJ, Martin LJ (2001) Early Neurodegeneration after Hypoxia-Ischemia in Neonatal Rat Is Necrosis while Delayed Neuronal Death Is Apoptosis. Neurobiol Dis 8:207–219.

Northington FJ, Graham EM, Martin LJ (2005) Apoptosis in perinatal hypoxic-ischemic brain injury: how important is it and should it be inhibited? Brain Res Brain Res Rev 50:244–257.

Ouyang YB, Tan Y, Comb M, Liu CL, Martone ME, Siesjö BK, Hu BR (1999) Survival- and death-promoting events after transient cerebral ischemia: phosphorylation of Akt, release of cytochrome C and Activation of caspase-like proteases. J Cereb Blood Flow Metab 19:1126–1135.

Pozo Devoto VM, Chavez JC, Fiszer de Plazas S (2006) Acute hypoxia and programmed cell death in developing CNS: Differential vulnerability of chick optic tectum layers. Neuroscience 142:645–653.

Rees S, Mallard C, Breen S, Stringer M, Cock M, Harding R (1998) Fetal brain injury following prolonged hypoxemia and placental insufficiency: a review. Comp Biochem Physiol A 119:653–660.

Rodríguez Gil DJ, Viapiano MS, Fiszer de Plazas S (2000) Acute hypoxic hypoxia transiently reduces GABA(A) binding site number in developing chick optic lobe. Brain Res Dev Brain Res 124:67–72.

Saggu SK, Chotaliya HP, Blumbergs PC, Casson RJ (2010) Wallerian-like axonal degeneration in the optic nerve after excitotoxic retinal insult: an ultrastructural study. BMC Neurosci 11:97.

Schwartz ML, Vaccarino F, Chacon M, Yan WL, Ment LR, Stewart WB (2004) Chronic neonatal hypoxia leads to long term decreases in the volume and cell number of the rat cerebral cortex. Semin Perinatol 28:379–388.

Schweichel JU, Merker HJ (1973) The morphology of various types of cell death in prenatal tissues. Teratology 7:253–266.

Scicolone GG, Pereyra-Alfonso SS, Brusco AA, Saavedra JJP, Flores VV (1995) Development of the laminated pattern of the chick tectum opticum. Int J Dev Neurosci 13:845–858.

Segura MF, Solé C, Pascual M, Moubarak RS, Perez-Garcia MJ, Gozzelino R, Iglesias V, Badiola N, Bayascas JR, Llecha N, Rodriguez-Alvarez J, Soriano E, Yuste VJ, Comella JX (2007) The long form of Fas apoptotic inhibitory molecule is expressed specifically in neurons and protects them against death receptor-triggered apoptosis. J Neurosci 27:11228–11241.

Shaham S, Horvitz HR (1996) Developing Caenorhabditis elegans neurons may contain both cell-death protective and killer activities. Genes Dev 10:578–591.

Wang J-Y, Xia Q, Chu K-T, Pan J, Sun L-N, Zeng B, Zhu Y-J, Wang Q, Wang K, Luo B-Y (2011) Severe global cerebral ischemia-induced programmed necrosis of hippocampal CA1 neurons in rat is prevented by 3-methyladenine: a widely used inhibitor of autophagy. J Neuropathol Exp Neurol 70:314–322.

Wei L, Ying D-J, Cui L, Langsdorf J, Yu SP (2004) Necrosis, apoptosis and hybrid death in the cortex and thalamus after barrel cortex ischemia in rats. Brain Res 1022:54–61.

Young C, Tenkova T, Dikranian K, Olney JW (2004) Excitotoxic versus apoptotic mechanisms of neuronal cell death in perinatal hypoxia/ischemia. Curr Mol Med 4:77–85.

Zhang Z, Galileo DS (1998) Widespread programmed cell death in early developing chick optic tectum. NeuroReport 9:2797–2801.

(Accepted 29 July 2013)
(Available online 8 August 2013)